Since January 2020 Elsevier has created a COVID-19 resource centre with free information in English and Mandarin on the novel coronavirus COVID-19. The COVID-19 resource centre is hosted on Elsevier Connect, the company's public news and information website.

Available online at www.sciencedirect.com

Respiratory Investigation

journal homepage: www.elsevier.com/locate/resinv

Original article

Chest CT severity score and radiological patterns as predictors of disease severity, ICU admission, and viral positivity in COVID-19 patients

Ioannis Bellos [a], *Kyriaki Tavernaraki* [b,*], *Konstantinos Stefanidis* [c], *Olympia Michalopoulou* [a], *Giota Lourida* [a], *Eleni Korompoki* [d], *Ioanna Thanou* [b], *Loukas Thanos* [b], *Angelos Pefanis* [a], *Aikaterini Argyraki* [a]

[a] *First Department of Internal Medicine and Infectious Diseases, "Sotiria" General and Chest Diseases Hospital of Athens, Greece*

[b] *Department of Imaging and Interventional Radiology, "Sotiria" General and Chest Diseases Hospital of Athens, Greece*

[c] *Radiology Department, King's College Hospital, London, United Kingdom*

[d] *Department of Clinical Therapeutics, National and Kapodistrian University of Athens, "Alexandra" General Hospital of Athens, Greece*

ARTICLE INFO

Article history:
Received 27 November 2020
Received in revised form
12 February 2021
Accepted 16 February 2021
Available online 19 March 2021

Keywords:
COVID-19
Computed tomography
Chest
Predict
Critical illness

ABSTRACT

Background: Chest computed tomography (CT) is a useful tool for the diagnosis of coronavirus disease-2019 (COVID-19), although its exact value for predicting critical illness remains unclear. This study evaluated the efficacy of chest CT to predict disease progression, pulmonary complications, and viral positivity duration.

Methods: A single-center cohort study was conducted by consecutively including hospitalized patients with confirmed COVID-19. The chest CT patterns were described and a total severity score was calculated. The predictive accuracy of the severity score was evaluated using the receiver operating characteristic analysis, while a Cox proportional hazards regression model was implemented to identify the radiological features that are linked to prolonged duration of viral positivity.

Results: Overall, 42 patients were included with 10 of them requiring intensive care unit admission. The most common lesions were ground glass opacities (92.9%), consolidation (66.7%), and crazy-paving patterns (61.9%). The total severity score significantly correlated with inflammatory and respiratory distress markers, as well as with admission CURB-65 and PSI/PORT scores. It was estimated to predict critical illness with a sensitivity and specificity of 75% and 70%, respectively. Time-to-event analysis indicated that patients

Abbreviations: SARS-CoV-2, severe acute respiratory syndrome coronavirus-2; COVID-2019, Coronavirus disease-2019; CT, computed tomography; ACE2, angiotensin-converting enzyme 2; ARDS, acute respiratory distress syndrome; CURB, Confusion, Urea, Respiratory rate, Blood pressure; PSI/PORT, Pneumonia Severity Index/Pneumonia Outcome Research Trial; MEWS, Modified Early Warning Score; SOFA, Sequential Organ Failure Assessment; APACHE II, Acute Physiology and Chronic Health Evaluation II; GGO, ground glass opacity; ROC, receiver operating characteristics; AUC, area under the curve.

* *Corresponding author*. Consultant Radiologist 152, Mesogion str, Athens, 115 27, Greece.
E-mail address: sandytavernaraki@hotmail.com (K. Tavernaraki).

https://doi.org/10.1016/j.resinv.2021.02.008

without ground-glass opacities presented significantly shorter median viral positivity (16 *vs.* 27 days).

Conclusions: Chest CT severity score positively correlates with markers of COVID-19 severity and presents promising efficacy in predicting critical illness. It is suggested that ground-glass opacities are linked to prolonged viral positivity. Further studies should confirm the efficacy of the severity score and elucidate the long-term pulmonary effects of COVID-19.

1. Introduction

Coronavirus disease-2019 (COVID-19) represents an emerging, potentially life-threatening, respiratory syndrome caused by severe acute respiratory syndrome coronavirus-2 (SARS-CoV-2), a betacoronavirus fist recognized in Wuhan, China [1]. It is mainly transmitted by respiratory droplets with a mean incubation time of five days, while pre-symptomatic carriers are suggested to contribute significantly to the disease spread [2]. Viral cell entry is based on the binding of its spike protein to the angiotensin-converting enzyme 2 (ACE2) receptor, which is mainly expressed by type II alveolar epithelial cells [3]. COVID-19 may range from asymptomatic disease to acute respiratory distress syndrome (ARDS), sepsis, and multiorgan failure, depending on patients' age, comorbidities, and host immune response [4]. Moreover, the disease may be linked to a hypercoagulable state, which may lead to arterial and venous thrombotic complications and even diffuse intravascular coagulation [5]. Various treatment strategies have been proposed, with promising evidence supporting the potential efficacy of dexamethasone [6] in reducing COVID-19-related mortality and remdesivir [7] in shortening the time to recovery in hospitalized patients.

Effective risk stratification is essential to guide clinical decisions regarding patient triaging and allocation of healthcare resources. To this point, much research effort has been devoted to the development of prognostic scores aiming to identify COVID-19 patients at increased risk of complications early during the course of the disease [8]. In this context, various predictive models have been constructed including several demographical and laboratory parameters, such as age, sex, comorbidities, lymphopenia, elevated D-dimers, and inflammatory markers [9]. However, the existing models have been criticized for being at high risk of bias, and lacking external validation; hence, no single clinical score is currently recommended to be widely applied in the clinical setting [10].

Chest computed tomography (CT) represents a useful tool for the initial evaluation of patients with suspected SARS-CoV-2 infection, presenting high sensitivity for the diagnosis of the disease [11]. Diffuse ground-glass opacities have been suggested as the hallmark of COVID-19, while several atypical manifestations have been also reported [12]. Ground-glass opacities as a radiological feature is non-specific for COVID-19, though it is typical and highly suggestive for the disease, especially when noted bilaterally and in the peripheral, subpleural location. This probably explains the low sensitivity of chest radiography for the depiction of lung changes during the early stages of the disease. The extent, distribution, and morphology of ground-glass opacities may vary on chest CT; therefore, diffuse, confluent, or patchy areas of ground glass may be observed as well as round-shaped. Furthermore, ground-glass opacities admixed with consolidation, as well as ground glass opacities with superimposed interlobular septal thickening, resulting in a crazy-paving pattern, have been described as frequent but non-specific radiological findings of COVID-19 pneumonia [13,14].

Nonetheless, the exact efficacy of chest CT in the prediction of disease progression remains still under investigation. The aim of the present study is to describe the time course of lung lesions on chest CT among COVID-19 individuals, as well as to assess the accuracy of a chest CT severity score for the prediction of critical illness. In addition, the role of chest CT in the detection of pulmonary complications, as well as the association of imaging findings with the duration of viral positivity are also evaluated.

2. Materials and methods

2.1. Study design and participants

The present cohort study was approved by the institutional review board of our institution ("Sotiria" Chest Diseases General Hospital, University of Athens, March 2020). Informed consent was obtained by all patients or their next of kin. A total of 42 patients with confirmed COVID-19 infection were consecutively enrolled. The diagnosis was solely based on the detection of SARS-CoV-2 by real-time reverse transcription polymerase chain reaction (rRT-PCR) analysis of nasopharyngeal swabs. All patients had at least one chest CT scan upon admission; selected cases had also a follow-up scan based on clinical indication. CT scans were categorized in four groups based on their timing: group 1 (CT performed 0–9 days after symptom onset), group 2 (CT performed 10–19 days after symptom onset), group 3 (CT performed 20–29) days after symptom onset) and group 4 (CT performed $\geq$ 30 days after symptom onset).

Information regarding patients' comorbidities (hypertension, diabetes mellitus, heart failure, chronic obstructive pulmonary disease, asthma, cancer, or immunodeficiency), symptoms, and clinical and laboratory characteristics were collected. Two pneumonia severity scores (Confusion, Urea, Respiratory rate, Blood pressure, age $\geq$ 65 years-CURB-65 [15]

and Pneumonia Severity Index/Pneumonia Outcome Research Trial-PSI/PORT [16]) were calculated at admission aiming to predict the risk of complications, while the maximum scores of Modified Early Warning Score (MEWS) [17], Sequential Organ Failure Assessment (SOFA) [18], and Acute Physiology and Chronic Health Evaluation II (APACHE II) [19] were estimated in order to identify critical illness. Duration of SARS-CoV-2 positivity was measured from the first day of symptoms (or the day of molecular diagnosis when the first day of symptoms was not available) to the day of the first negative nasopharyngeal swab. All data were collected by two researchers independently, while any potential discrepancies were resolved by their consensus or discussion with all authors.

2.2. CT image acquisition technique

Chest CT scans were performed using a 16-Slice CT Scanner (GE Medical Systems, Optima CT540) with 2.5-mm section thickness, 1.25-mm reconstruction slice thickness, and 120 KVp tube voltage. Non-contrast chest CT scan was obtained with the patient in supine position and at end-inspiration when possible, while a dedicated CT Pulmonary Angiography protocol with bolus tracking was acquired in cases of suspected pulmonary embolism.

2.3. Image interpretation

Two senior chest radiologists (14 and 15 years of experience) evaluated separately all CT images, without access to the clinical or laboratory characteristics of patients. The presence of the following radiological lesions and patterns was retrospectively assessed [20]: ground-glass opacity (GGO), consolidation, GGO with consolidation, round GGO, crazy-paving, organizing pneumonia pattern, interlobular septal thickening, parenchymal bands, halo sign, reverse halo sign, air-bronchogram, traction bronchiectasis, cavitation, nodules, subsegmental vessel enlargement, pleural effusion, and lymphadenopathy. In addition, the location (unilateral/bilateral), distribution (peripheral/peribronchovascular), zonal predominance (upper/mid/lower), and the lung background (normal/emphysema/fibrosis) were evaluated. Potential complications, especially pulmonary embolism, radiological signs of bacterial superinfection, mainly consolidation in a specific lobe or lung segment, mucoid impactions, centrilobular nodules with tree-in-bud and cavitation, as well as predictive signs of pulmonary fibrosis including a combination of traction bronchiectasis, parenchymal bands, and atelectasis were also taken into account.

A chest CT severity score was calculated by assessing the degree of lobe involvement for each of the five lung lobes separately as follows: 0% (no involvement), 1%–25% (minimal involvement), 26%–50% (mild involvement), 51%–75% (moderate involvement), and 76%–100% (severe involvement). Corresponding scores for each degree of lobe involvement were classified from lobe score 0 (no involvement) to lobe score 4 (severe involvement). The overall lung "total severity score" was calculated by adding the five lobe scores reaching a range of possible scores from 0 to 20 [21]. Follow-up CT scans were judged to show progression, resolution, or no change of pulmonary lesions. Any disagreements between the two radiologists were resolved through their consensus.

2.4. Data analysis

Statistical analysis was performed in R-3.6.3. The threshold of a two-sided *p-value* < 0.05 was chosen to define statistical significance. Inter-rater agreement was judged by estimating the Cohen's *kappa* (κ) coefficient [22]. Patients were categorized depending on whether they were admitted to the intensive care unit (ICU), while CT scans were classified based on their timing since symptom onset. The normality of continuous variables was tested by the Shapiro-Wilk test [23]. Normally distributed data were expressed as mean and standard deviation and were compared using the Student's *t-test*. Otherwise, the median and interquartile range were reported and comparisons were conducted with the Mann-Whitney *U-test*. The Fischer's exact test was used for the analysis of binary variables, while comparisons of three or more groups were performed with the one-way analysis of variance method or the Kruskal-Wallis test, as appropriate [24]. The potential correlations of the chest CT severity score with inflammatory (white blood cells, neutrophil-to-lymphocyte ratio, C-reactive protein, procalcitonin, ferritin and fibrinogen) and respiratory distress markers (PaO_2/FiO_2 ratio and arterial-alveolar gradient), as well as with clinical scores (initial CURB-65 and PSI/PORT, worst MEWS, SOFA, and APACHE II) were tested using the Pearson or the non-parametric Spearman correlation coefficients, depending on the normality of the data [25]. Multiplicity correction was performed via false discovery rate estimation following the Benjamini-Hochberg method.

The accuracy of the chest CT severity score in the prediction ICU admission was evaluated by constructing the receiver operating characteristics (ROC) curve and calculating the area under the curve (AUC). Only the initial CT scans were taken into consideration for the diagnostic accuracy analysis in order to ensure the predictive nature of the CT score measurements. The optimal threshold was identified by calculating the Youden index [26], and the corresponding sensitivity and specificity were reported. Moreover, ROC analysis was planned to be implemented, aiming to assess the efficacy of maximum C-reactive protein and procalcitonin in predicting bacterial superinfection, as detected by chest CT imaging. A time-to-event analysis was also conducted by applying a Cox proportional hazards regression model, aiming to identify which radiological features are associated with prolonged SARS-CoV-2 positivity.

3. Results

3.1. Clinical characteristics

A total of 42 patients were included and 10 of them were admitted to the ICU, requiring invasive mechanical ventilation. The clinical and laboratory characteristics of the participants are summarized in Table 1. Specifically, 29 patients (69%) were males, while the mean age of the study population was 56.64 years (SD: 14.12, range: 33 to 92). The most common

Table 1 – Clinical and laboratory characteristics of the study population.

Clinical characteristics	All patients (*N* = 42)	Admission to ICU		*p-value*
		Yes (N = 10)	No (N = 32)	
Age (years)	56.64±14.12	61.30±8.51	55.19±15.28	0.120
Male gender	29 (69.0%)	9 (90%)	20 (62.5%)	0.134
Obesity	12 (28.6%)	4 (40%)	8 (25%)	0.433
Smoking history	11 (26.2%)	4 (40%)	7 (21.9%)	0.418
Comorbidities				
Hypertension	12 (28.6%)	6 (60%)	6 (18.8%)	**0.019**
Diabetes mellitus	2 (4.8%)	2 (20%)	0 (0%)	0.052
Heart failure	1 (2.4%)	0 (0%)	1 (3.1%)	1
Chronic kidney disease	4 (9.5%)	1 (10%)	3 (9.4%)	1
Chronic obstructive pulmonary disease	1 (2.4%)	0 (0%)	1 (3.1%)	1
Asthma	4 (9.5%)	1 (10%)	3 (9.4%)	1
Cancer	2 (4.8%)	0 (0%)	2 (6.3%)	1
Immunodeficiency	2 (4.8%)	1 (10%)	1 (3.1%)	0.424
Symptoms				
Fever	41 (97.6%)	10 (100%)	31 (96.9%)	1
Cough	28 (66.7%)	5 (50%)	23 (71.9%)	0.241
Fatigue	26 (61.9%)	4 (40%)	22 (68.8%)	0.130
Shortness of breath	25 (59.5%)	9 (90%)	16 (50%)	**0.031**
Diarrhea	13 (30.9%)	0 (0%)	13 (40.6%)	**0.018**
Vomiting	4 (9.5%)	2 (20%)	2 (6.3%)	0.245
Loss of smell	4 (9.5%)	0 (0%)	4 (12.5%)	0.556
Vital signs – Arterial blood gases at admission				
Mean arterial pressure (mmHg)	90 [80.83–95.83]	93.33 [83.33–99.17]	89.17 [80–93.33]	0.458
Heart rate (beats/minute)	81.88±14.55	89.11±15.89	79.84±13.73	0.139
PaO_2/FiO_2 ratio (mmHg)	340.9 [288.7–376.5]	220 [190.6–271.4]	361.9 [328.6–388.1]	**<0.001**
Arterial-alveolar gradient (mmHg)	37.93 [30.93–68.93]	130.85 [60.09–160.45]	36.73 [27.84–42.03]	**0.002**
Lactate (mmol/L)	1.14±0.32	1.23±0.30	1.12±0.32	0.350
Laboratory tests at admission				
White blood cells (/μL)	6572±2518	6807±3586	6499±2152	0.801
Neutrophils (/μL)	4457±1997	5258±2954	4206±1571	0.304
Lymphocytes (/μL)	1335 [922–1875]	1214 [741–1560]	1500 [950–1912]	**<0.001**
Neutrophil-to-lymphocyte ratio	3.04 [1.88–4.72]	4.15 [3.04–4.55]	3.01 [1.63–3.96]	0.090
Platelets (/μL)	197.29±64.85	174.97±60.94	204.27±65.37	0.211
Platelet-to-lymphocyte ratio	216 [160.5–394.5]	202.69 [175.3–249.07]	260.3 [159.8–449.6]	0.163
Hemoglobin (g/dL)	13.96±1.26	14.39±1.48	13.82±1.18	0.288
C-reactive protein (mg/dL)	6.4 [1.34–10.90]	12.52 [6.72–15.95]	3.34 [1.15–10.24]	**0.024**
Procalcitonin (ng/mL)	0.09 [0.04–0.13]	0.13 [0.10–0.20]	0.04 [0.03–0.11]	**0.011**
Ferritin (ng/mL)	496.2 [245–949.25]	989 [682.2–2259.5]	434.8 [188–833]	**0.025**
Lactate dehydrogenase (U/L)	265 [219–365]	359 [262.2–384.1]	258 [206.5–348]	0.071
Urea (mg/dL)	28.5 [23.25–37.5]	35 [30.5–50]	28 [22.75–33]	0.065
Creatinine (mg/dL)	0.9 [0.8–1.0]	1.0 [0.9–1.08]	0.9 [0.8–1.0]	0.062
Aspartate aminotransferase (U/L)	33 [24.5–43.75]	47 [31–68]	30.5 [22.75–43]	**0.035**
Alanine aminotransferase (U/L)	33.5 [21–54]	46.5 [24.25–62.75]	33 [21–45.5]	0.330
Total bilirubin (mg/dL)	0.6 [0.48–0.8]	0.6 [0.53–0.68]	0.6 [0.43–0.8]	0.875
Fibrinogen (mg/dL)	563.9±169.8	673.7±156.7	525.9±159.7	**0.029**
D-dimers (μg/mL)	0.56 [0.38–1.31]	0.74 [0.64–1.20]	0.49 [0.32–1.61]	0.249
Treatment				
Oseltamivir	16 (38.1%)	5 (50%)	11 (34.4%)	0.465
Hydroxychloroquine	31 (73.8%)	10 (100%)	21 (65.6%)	**0.041**
Azithromycin	32 (76.2%)	10 (100%)	22 (68.8%)	0.084
Ceftriaxone	17 (40.5%)	7 (70%)	10 (31.3%)	0.062
Clinical scores				
Initial CURB-65	1 [0–1]	2 [1,2]	0 [0–1]	**<0.001**
Initial PSI/PORT	68 [52–81]	74.5 [71.5–111]	58 [47–78]	**0.005**
Maximum MEWS	1 [0–2]	3 [2–4]	1 [0–2]	**<0.001**
Maximum SOFA	2 [1–3]	3 [3–3]	2 [1,2]	**0.001**
Maximum APACHE II	6.5 [3.75–9]	11 [9–11]	5 [2–7.5]	**<0.001**

Bold text indicates statistical significance (p-value <0.05). Continuous data are expressed as mean ± standard deviation or median [interquartile range].

comorbidity was hypertension (28.6%), while the most prevalent symptoms were fever (97.6%) and cough (66.7%), followed by fatigue (61.9%) and shortness of breath (59.5%). Patients who were subsequently admitted to the ICU presented at hospital admission significantly lower PaO_2/FiO_2 ratio (*p-value* < 0.001) and higher arterial-alveolar gradient (*p-value*: 0.002), as well as lower lymphocyte count (*p-value* < 0.001) and higher serum C-reactive protein (*p-value*: 0.024), procalcitonin (*p-value*: 0.011), ferritin (*p-value*: 0.025), aspartate aminotransferase (*p-value*: 0.035), and fibrinogen (*p-value*: 0.029). In addition, critically-ill ICU patients had significantly higher initial CURB-65 (*p-value* < 0.001) and PSI/PORT (*p-value*: 0.005) scores, as well as significantly higher maximum values of MEWS (*p-value* < 0.001), SOFA (*p-value*: 0.001), and APACHE II (*p-value* < 0.001) scores.

3.2. *Radiological findings*

Inter-rater agreement was assessed to be strong, as the estimated values of Cohen's *kappa* were found to be > 0.8 in all outcomes (Suppl. Table 1). The radiological features of patients are presented in Table 2. Evaluation of pulmonary background revealed normal lung in 88.1% of cases, while emphysema was detected in three patients (7.1%). In the majority of patients, lesions were present bilaterally (92.9%), affecting predominantly the lower lobes in 61.9% of cases. Peripheral and peribronchovascular distribution were detected in 30.9% and 4.8% of patients, respectively, while both patterns were present in 24 individuals (57.1%) (Fig. 1). The most common types of lesions were GGO (92.9%), consolidation (66.7%), crazy-paving (61.9%), interlobular septal

Table 2 – Chest CT findings of the included patients.

Radiological characteristics	All patients (N = 42)	Admission to ICU		*p-value*
		Yes (N = 10)	No (N = 32)	
Background				
Normal lung	37 (88.1%)	8 (80%)	29 (90.6%)	0.341
Emphysema	3 (7.1%)	1 (10%)	2	
Fibrosis	1 (2.4%)	1 (10%)	0	
Emphysema + fibrosis	1 (2.4%)	0 (0%)	1	
Location				
Unilateral	0 (%)	0 (%)	0 (%)	1
Bilateral	39 (92.9%)	10 (100%)	29 (90.6%)	
No. of affected lobes	5 [4,5]	5 [5–5]	5 [3–5]	0.080
Distribution				
Peripheral	13 (30.9%)	0 (0%)	13 (40.6%)	**0.015**
Peribronchovascular	2 (4.8%)	1 (10%)	1 (3.1%)	
Both	24 (57.1%)	9 (90%)	15 (46.9%)	
Zonal predominance				
No predominance	7 (16.7%)	2 (20%)	5 (15.6%)	1
Upper	7 (16.7%)	2 (20%)	5 (15.6%)	
Mid	2 (4.8%)	0 (0%)	2 (6.3%)	
Lower	26 (61.9%)	6 (60%)	20 (62.5%)	
Pattern of lesions				
Ground glass opacity	39 (92.9%)	10 (100%)	29 (90.6%)	1
Consolidation	28 (66.7%)	7 (70%)	21 (65.6%)	1
Crazy paving	26 (61.9%)	8 (10%)	18 (56.3%)	0.270
Interlobular septal thickening	25 (59.5%)	8 (80%)	17 (53.1%)	0.162
Parenchymal bands	23 (54.8%)	7 (70%)	16 (50%)	0.305
Ground glass opacity with consolidation	21 (50%)	7 (70%)	14 (43.8%)	0.277
Organizing pneumonia pattern	20 (47.6%)	3 (30%)	17 (53.1%)	0.284
Traction bronchiectasis	19 (45.2%)	7 (70%)	12 (37.5%)	0.144
Round ground glass opacity	11 (26.2%)	1 (10%)	10 (23.8%)	0.245
Pleural effusion	9 (21.4%)	2 (20%)	7 (21.9%)	1
Lymphadenopathy	10 (23.8%)	2 (20%)	8 (25%)	0.181
Air-bronchogram	4 (9.5%)	2 (20%)	2 (6.3%)	0.236
Reverse halo sign	3 (7.1%)	0 (0%)	3 (9.4%)	1
Halo sign	1 (2.4%)	0 (0%)	1 (3.1%)	1
Nodules	1 (2.4%)	0 (0%)	1 (3.1%)	1
Cavitation	0 (0%)	0 (0%)	0 (%)	N/A
Subsegmental vessel enlargement	0 (0%)	0 (0%)	0 (%)	N/A
Complications				
Radiological superinfection	5 (11.9%)	2 (20%)	3 (9.4%)	0.577
Pulmonary embolism	3 (7.1%)	3 (30%)	0 (0%)	**0.010**
Signs predictive of fibrosis	22 (52.4%)	9 (90%)	13 (40.6%)	**0.010**
Severity score	11.75±4.75	12.60±4.25	7.38±4.23	**0.004**

Bold text indicates statistical significance (p-value <0.05).Continuous data are expressed as mean ± standard deviation or median [interquartile range].

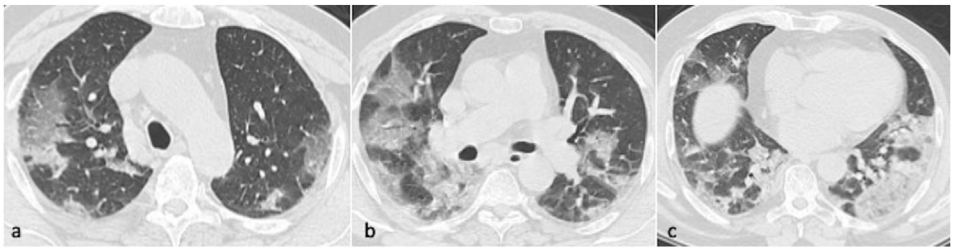

Fig. 1 – Axial CT chest images in a 57-year-old male patient in the upper, mid and lower zones showing extensive, bilateral predominantly ground glass opacities in peripheral and peribronchovascular distribution. Estimated total CT severity score 18.

thickening (59.5%), parenchymal bands (54.8%), GGO with consolidation (50%), organizing pneumonia pattern (47.6%), and traction bronchiectasis (45.2%). Less common findings were round GGO (26.2%), pleural effusion (21.4%), lymphadenopathy (23.8%), air-bronchogram (9.5%), reverse halo sign (7.1%), halo sign (2.4%), and nodules (2.4%). Patients admitted to the ICU presented significantly higher rates of both peripheral and peribronchovascular distribution of lesions (*p-value*: 0.015), as well as a higher risk of observing sings predictive of pulmonary fibrosis (*p-value*: 0.01). Pulmonary embolism was observed in three cases after admission to the ICU (*p-value*: 0.01).

3.3. *Time course*

Totally, 14 follow-up CT scans were performed, with seven of them showing progression, two regression, and five no significant change of pulmonary lesions. The time course of lung changes is depicted in Fig. 2. GGO was the most prevalent type of lesion during all phases of the infection. On the other hand, late stages of the disease were linked to significantly lower rates of crazy-paving (*p-value*: 0.002), interlobular septal thickening (*p-value*: 0.023), and round GGO (*p-value*: 0.015). It should be noted that the proportion of patients showing radiological signs predictive of pulmonary fibrosis was highest (83.3%) in group 4 (≥30 days from symptom onset) (Suppl. Table 2).

3.4. *Chest CT severity score*

The mean chest CT severity score was estimated to be 11.75 (SD: 4.75, range: 0–18). Patients developing critical illness presented significantly higher chest CT severity scores (12.60 ± 4.25 vs. 7.38 ± 4.23, *p-value*: 0.004). The AUC of the chest CT severity score for the prediction of ICU admission was calculated to be 81.1%; hence, the marker was estimated to provide a sensitivity of 75% and specificity of 70% at the threshold of 10.5 (Fig. 3). Moreover, significant correlation was observed between chest CT severity score and PaO_2/FiO_2 ratio (*r*: 0.555, *p-value* < 0.001), arterial-alveolar gradient (*r*: 0.458, *p-value*: 0.004), blood lactate (*r*: 0.433, *p-value*: 0.007), serum C-reactive protein (*r*: 0.694, *p-value* < 0.001), ferritin (*r*: 0.487, *p-value*: 0.007), fibrinogen (*r*: 0.474, *p-value*: 0.006), neutrophil-to-lymphocyte ratio (*r*: 0.411, *p-value*: 0.008), initial CURB-65 (*r*: 0.581, *p-value* < 0.001), and PSI/PORT scores (*r*: 0.512, *p-value* < 0.001), as well as with worst MEWS (*r*: 0.560, *p-value* < 0.001), SOFA (*r*: 0.470, *p-value*: 0.004), and APACHE II (*r*: 0.576, *p-value* <0.001) scores (Fig. 4). No significant correlation of chest CT severity score with white blood cell count (*r*: 0.105, *p-value*: 0.507) and procalcitonin (*r*: 0.204, *p-value*: 0.234) was estimated. A correlation matrix is depicted in Suppl. Fig. 1.

3.5. *Bacterial superinfection*

Bacterial superinfection was suspected by chest CT in nine cases (5 initial and 4 follow-up scans). Of them, the infection was microbiologically confirmed in five patients, with *Acinetobacter baumannii* being isolated in sputum in four cases and *Klebsiella pneumoniae* in one case. The diagnostic accuracy of maximum C-reactive protein and procalcitonin for the detection of radiological superinfection was estimated to be moderate (AUC: 74.1% and 70.3%, respectively). Specifically, C-reactive protein provided a sensitivity of 88.9% and specificity of 62.5% at the optimal threshold of 21.5 mg/L, while both the sensitivity and specificity of procalcitonin were calculated to be 75% at the cut-off of 0.2 ng/mL (Suppl. Fig. 2).

3.6. *Duration of viral positivity*

The median duration of SARS-CoV-2 positivity for the entire cohort was 25 days (95% confidence intervals-CI: 23 to 32) from the 1st day of symptoms. Univariate Cox proportional hazard regression analysis indicated that the only radiological feature associated with prolonged viral positivity was the presence of ground-glass opacities. No significant association with positivity duration was estimated for age, sex, consolidation, ground-glass opacities with consolidation, parenchymal bands, crazy paving, air bronchogram, round ground glass opacity, septal thickening, organizing pneumonia pattern, pleural effusion, or bacterial superinfection pattern (Suppl. Table 3). Therefore, as it is evident from the Kaplan-Meier curve, cases without ground-glass opacities on the admission chest CT presented significantly shorter median viral positivity (16 *vs.* 27 days, hazard ratio: 0.08, 95% CI: 0.02 to 0.35, *p-value* < 0.001) (Suppl. Fig. 3).

4. Discussion

The present study evaluated the imaging findings of patients with laboratory-confirmed SARS-CoV-2 infection in order to assess the role of chest CT in the prediction of disease

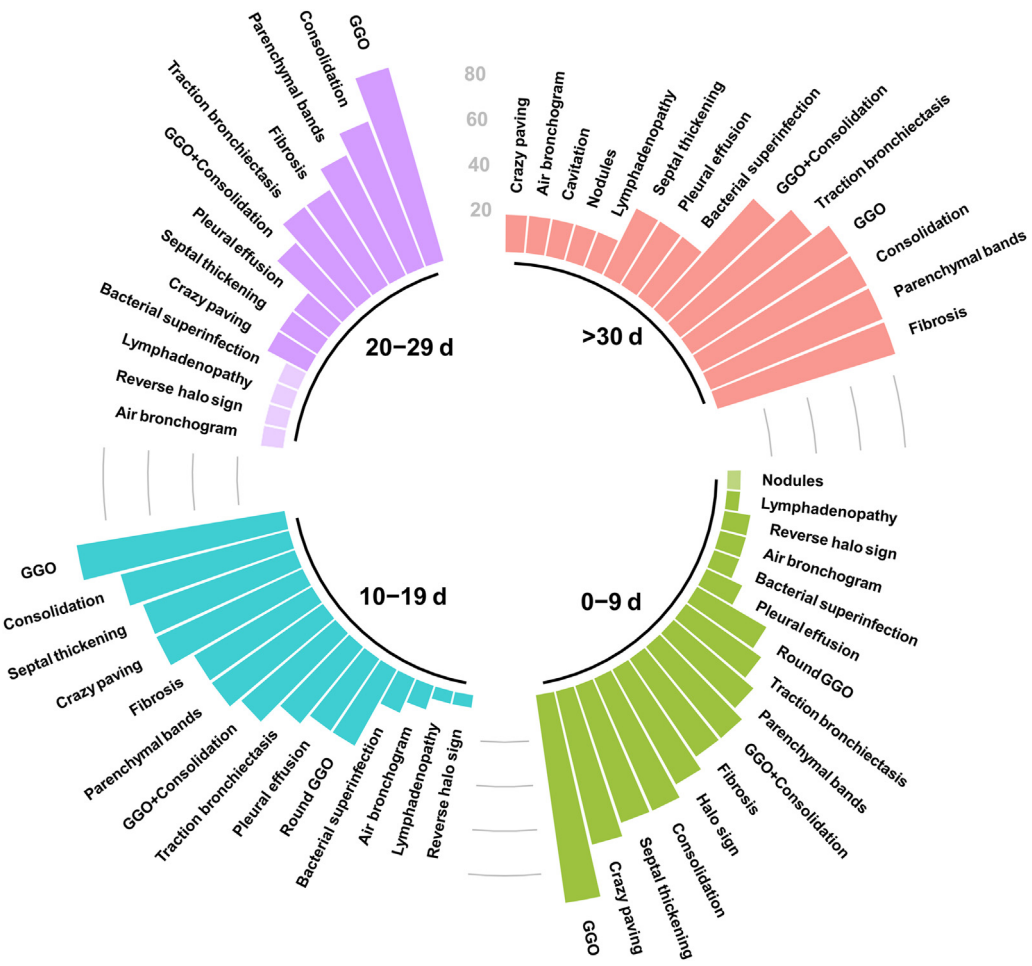

Fig. 2 – Frequency of lung changes at chest CT depending on the time of scan since symptom onset. Chest CT scans were categorized based on whether they were performed 0–9, 10–19, 20–29 or ≥30 days from symptoms onset.

progression and critical illness. To achieve this, the chest CT severity score was estimated and diagnostic accuracy analysis was performed, indicating promising efficacy of the score in the detection of patients prone to develop severe disease. This finding is in accordance with previous studies in the field [27,28], supporting the significant association of initial chest CT severity score with both short and long-term prognosis. Importantly, the chest CT score was suggested to positively correlate with admission inflammation markers (C-reactive protein, ferritin, neutrophil/lymphocyte ratio, fibrinogen), as well as with established clinical scores of pneumonia severity (CURB-65, PSI/PORT) and critical illness (MEWS, SOFA, APACHE II). In this context, it has been proposed that the extent of pulmonary lesions may reflect the degree of systemic inflammatory response, while preliminary data have indicated the potential beneficial effects of glucocorticoid therapy, leading to regression of lung infiltrates [29].

The majority of cases presented bilateral lung involvement, affecting mainly the lower lobes. Ground glass opacities and consolidations were the most prevalent lesions, especially during the initial phases of the disease. A crazy-paving pattern was commonly noticed during the first 20 days from symptom onset, while nodules, cavities, pleural effusion, and lymphadenopathy were rarely observed. Interestingly, the incidence of parenchymal bands and traction bronchiectasis was high in scans performed after 30 days from disease onset and thus indicative signs of pulmonary fibrosis were detected in the majority of patients during the late phase of the infection. This observation is in accordance with previous reports [30] and has been confirmed by recent autopsy findings, supporting that lung specimens obtained by patients who died after a long disease duration (i.e. > 30 days) presented pronounced histologic fibrotic remodeling [31]. However, whether COVID-19 may lead to long-term fibrosis and loss of pulmonary function remains to be determined by further longitudinal studies.

Sequential SARS-CoV-2 testing in nasopharyngeal swabs indicated that the duration of viral positivity was significantly shorter in patients without ground-glass opacities at admission. Moreover, the presence of ground-glass opacities was the only imaging feature associated with prolonged viral positivity. Previous studies have suggested that prolonged viral shedding may be linked to disease severity [32], as well as to higher levels of $CD8^{+}$ T-lymphocytes [33], although the exact factors associated with the duration of SARS-CoV-2 positivity remain currently unclear. In this context, the combination of clinical and radiological features may enable the identification of patients at risk of longer viral presence in

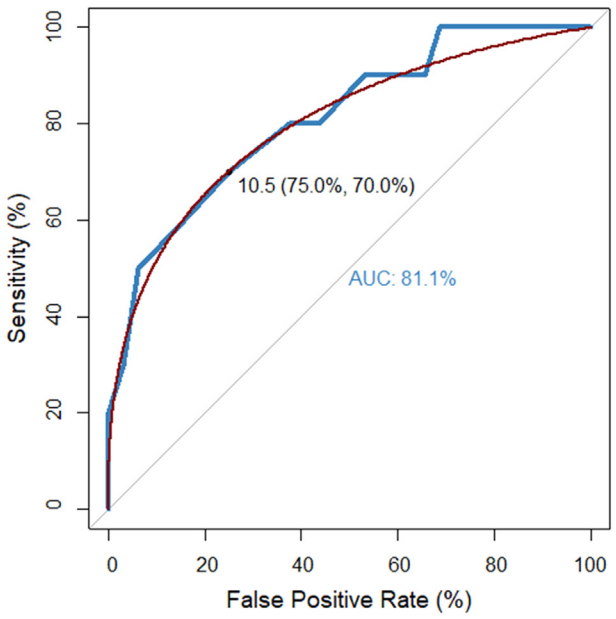

Fig. 3 – Receiver operating characteristics curve of chest CT severity score for the prediction of admission to the intensive care unit. The threshold of 10.5 provided sensitivity and specificity of 75% and 70%, respectively. ***AUC: area under the curve.***

order to guide decisions about self-isolation and discharge of hospitalized patients. Nonetheless, whether increased duration of SARS-CoV-2 positivity translates to prolonged infectivity and transmission risk remains to be elucidated.

The present study has several strengths. Data were registered in a comprehensive database, with radiologists being blinded to clinical and laboratory outcomes. Inter-rater agreement was high, supporting the robustness of radiological evaluations. Patient recruitment was consecutive and the examined variables and end-points were pre-specified; hence, the risk of selection bias was limited. To our knowledge, it is the first time that the relationship of chest CT features with the duration of viral shedding are assessed, suggesting that imaging may provide useful information about infectivity and contribute to the optimization of isolation strategies. Previous studies have demonstrated that prolonged viral shedding may be also associated with immunosuppression and elevated interleukin-6 levels [34], as well as with high viral load expressed as RNA copies. Conversely, detecting serum neutralizing antibody titer $\geq$1:20 has been linked to non-infectiousness [35]. On the other hand, the interpretation of outcomes is mainly limited by the available sample size; the study was a single-center one and thus generalizability of the results to populations of other countries cannot be ensured. In addition, only hospitalized patients were examined; hence, data from asymptomatic patients were not included in the analysis. It should be also noted that follow-up CT scans were performed by clinical indication and thus radiological information was not uniformly available during the late phase of the disease.

Several aspects remain to be clarified in order to shed light on the exact role of chest CT in the prediction of critical illness among COVID-19 patients. Specifically, the predictive accuracy of the chest CT severity score should be validated by further studies using predefined thresholds, based on the present outcomes. Moreover, the observed temporal changes of lung lesions should be confirmed by prospective cohorts performing CT scans at pre-specified time-points during the course of the disease. The long-term effects of COVID-19 on pulmonary parenchyma should be also assessed by examining whether the incipient fibrotic changes seen during the acute phase may lead to permanent interstitial lung disease. In addition, the influence of viral load on the radiological

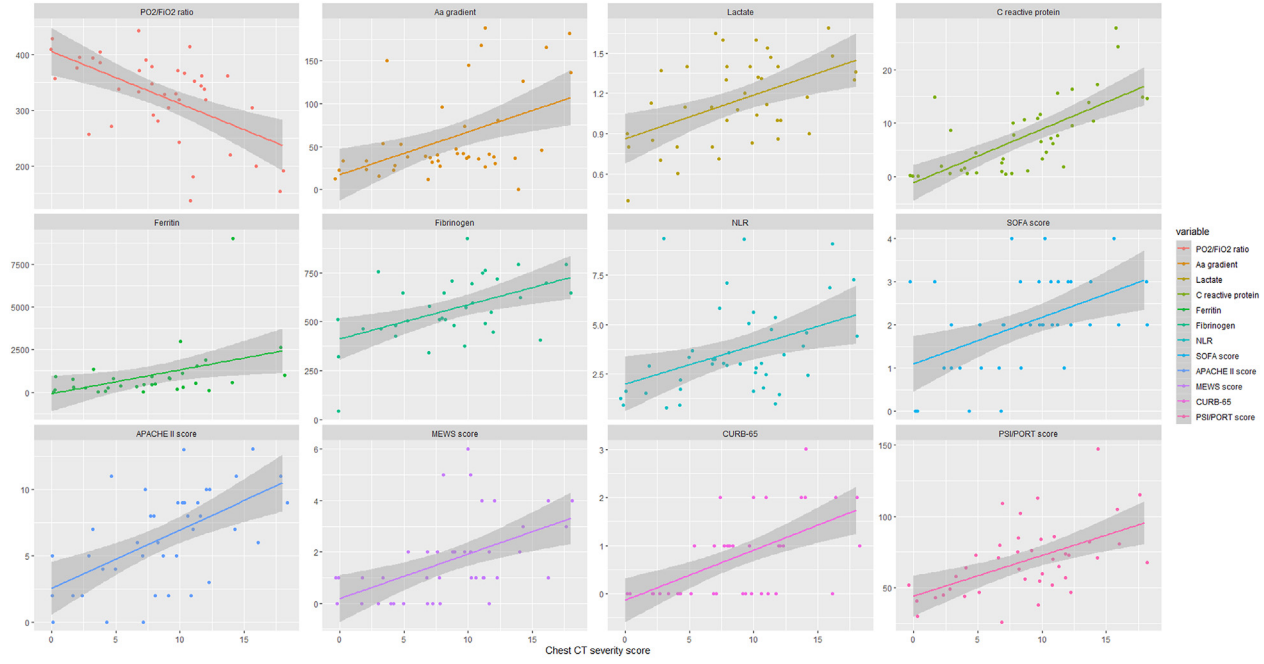

Fig. 4 – Correlation of chest CT severity score with clinical scores, inflammatory and respiratory distress markers. The horizontal x-axis depicts the chest CT severity score and the vertical y-axis shows the values of clinical markers.

appearance and severity of lung lesions may be further evaluated by methods allowing absolute viral quantification. Finally, it is important to combine chest CT findings with clinical and laboratory data aiming to construct multivariate predictive models, achieving optimal discrimination of patients at high risk of disease progression.

5. Conclusions

The present study suggests that chest CT severity score constitutes a useful tool for the initial evaluation of COVID-19 patients as it positively correlates with markers of disease severity and presents promising efficacy in the prediction of critical illness and ICU admission. The temporal changes of pulmonary lesions during the course of the disease were described, suggesting that the presence of ground glass opacities is the most prevalent radiological feature among hospitalized patients, predisposing for prolonged viral positivity. Parenchymal bands and traction bronchiectasis are increasingly observed during the late phases of the infection, although whether COVID-19 may lead to long-term pulmonary fibrosis remains to be elucidated.

Funding

This study was carried out as part of our routine work.

Conflict of Interest

The authors declare that they have no conflicts of interest.

Acknowledgements

None.

Appendix A. Supplementary data

Supplementary data to this article can be found online at https://doi.org/10.1016/j.resinv.2021.02.008.

REFERENCES

[1] Li Q, Guan X, Wu P, Wang X, Zhou L, Tong Y, et al. Early transmission dynamics in wuhan, China, of novel coronavirus-infected pneumonia. N Engl J Med 2020;382:1199–207. https://doi.org/10.1056/NEJMoa2001316.
[2] Jayaweera M, Perera H, Gunawardana B, Manatunge J. Transmission of COVID-19 virus by droplets and aerosols: a critical review on the unresolved dichotomy. Environ Res 2020;188:109819. https://doi.org/10.1016/j.envres.2020.109819.
[3] Yuki K, Fujiogi M, Koutsogiannaki S. COVID-19 pathophysiology: a review. Clin Immunol 2020;215:108427. https://doi.org/10.1016/J.CLIM.2020.108427.
[4] Cao W, Li T. COVID-19: towards understanding of pathogenesis. Cell Res 2020;30:367–9. https://doi.org/10.1038/s41422-020-0327-4.
[5] Becker RC. COVID-19 update: Covid-19-associated coagulopathy. J Thromb Thrombolysis 2020;50(1):54–67. https://doi.org/10.1007/S11239-020-02134-3.
[6] Recovery Collaborative Group H, Horby P, Lim WS, Emberson JR, Mafham M, Bell JL, et al. Dexamethasone in hospitalized patients with covid-19. N Engl J Med 2021;384:693–704. https://doi.org/10.1056/NEJMoa2021436.
[7] Beigel JH, Tomashek KM, Dodd LE, Mehta AK, Zingman BS, Kalil AC, et al. Remdesivir for the treatment of covid-19 — final report. N Engl J Med 2020;383:1813–26. https://doi.org/10.1056/nejmoa2007764.
[8] Wiersinga WJ, Rhodes A, Cheng AC, Peacock SJ, Prescott HC. Pathophysiology, transmission, diagnosis, and treatment of coronavirus disease 2019 (COVID-19). J Am Med Assoc 2020;324(8):782–93. https://doi.org/10.1001/jama.2020.12839.
[9] Wu C, Chen X, Cai Y, Xia J, Zhou X, Xu S, et al. Risk factors associated with acute respiratory distress syndrome and death in patients with coronavirus disease 2019 pneumonia in wuhan, China. JAMA Intern Med 2020;180:934. https://doi.org/10.1001/jamainternmed.2020.0994.
[10] Wynants L, Calster B Van, Collins GS, Riley RD, Heinze G, Schuit E, et al. Prediction models for diagnosis and prognosis of covid-19: systematic review and critical appraisal. BMJ 2020;369. https://doi.org/10.1136/BMJ.M1328.
[11] Xu B, Xing Y, Peng J, Zheng Z, Tang W, Sun Y, et al. Chest CT for detecting COVID-19: a systematic review and meta-analysis of diagnostic accuracy. Eur Radiol 2020;1. https://doi.org/10.1007/s00330-020-06934-2.
[12] Zheng Y, Wang L, Ben S. Meta-analysis of chest CT features of patients with COVID-19 pneumonia. J Med Virol 2020;93(1):241–9. https://doi.org/10.1002/jmv.26218. jmv.26218.
[13] Revel MP, Parkar AP, Prosch H, Silva M, Sverzellati N, Gleeson F, et al. COVID-19 patients and the radiology department – advice from the European society of radiology (ESR) and the European society of thoracic imaging (ESTI). Eur Radiol 2020;30:4903–9. https://doi.org/10.1007/s00330-020-06865-y.
[14] Simpson S, Kay FU, Abbara S, Bhalla S, Chung JH, Chung M, et al. Radiological society of north America expert consensus statement on reporting chest CT findings related to COVID-19. Endorsed by the society of thoracic radiology, the American college of radiology, and RSNA. Radiol Cardiothorac Imaging 2020;2:e200152. https://doi.org/10.1148/ryct.2020200152.
[15] Lim WS, van der Eerden MM, Laing R, Boersma WG, Karalus N, Town GI, et al. Defining community acquired pneumonia severity on presentation to hospital: an international derivation and validation study. Thorax 2003;58:377–82. https://doi.org/10.1136/thorax.58.5.377.
[16] Fine MJ, Auble TE, Yealy DM, Hanusa BH, Weissfeld LA, Singer DE, et al. A prediction rule to identify low-risk patients with community-acquired pneumonia. N Engl J Med 1997;336:243–50. https://doi.org/10.1056/NEJM199701233360402.
[17] Subbe CP, Kruger M, Rutherford P, Gemmel L. Validation of a modified early warning score in medical admissions. QJM 2001;94:521–6. https://doi.org/10.1093/qjmed/94.10.521.
[18] Vincent JL, Moreno R, Takala J, Willatts S, De Mendonça A, Bruining H, et al. The SOFA (Sepsis-related organ failure assessment) score to describe organ dysfunction/failure. On behalf of the working group on sepsis-related problems of the European society of intensive care medicine. Intensive Care Med 1996;22:707–10. https://doi.org/10.1007/BF01709751.
[19] Knaus W, Draper E, Wagner D, Zimmerman J. Apache II: a severity of disease classification system. Crit Care Med 1985;13:818–29.

[20] Hansell DM, Bankier AA, MacMahon H, McLoud TC, Müller NL, Remy J. Fleischner Society: glossary of terms for thoracic imaging. Radiology 2008;246:697–722. https://doi.org/10.1148/radiol.2462070712.
[21] Chung M, Bernheim A, Mei X, Zhang N, Huang M, Zeng X, et al. CT imaging features of 2019 novel coronavirus (2019-NCoV). Radiology 2020;295:202–7. https://doi.org/10.1148/radiol.2020200230.
[22] Cohen J. A coefficient of agreement for nominal scales. Educ Psychol Meas 1960;20:37–46. https://doi.org/10.1177/001316446002000104.
[23] Mishra P, Pandey CM, Singh U, Gupta A, Sahu C, Keshri A. Descriptive statistics and normality tests for statistical data. Ann Card Anaesth 2019;22:67–72. https://doi.org/10.4103/aca.ACA_157_18.
[24] Lantz B. The impact of sample non-normality on ANOVA and alternative methods. Br J Math Stat Psychol 2013;66:224–44. https://doi.org/10.1111/j.2044-8317.2012.02047.x.
[25] Schober P, Boer C, Schwarte LA. Correlation coefficients: appropriate use and interpretation. Anesth Analg 2018;126:1763–8. https://doi.org/10.1213/ANE.0000000000002864.
[26] Youden WJ. Index for rating diagnostic tests. Cancer 1950;3:32–5. https://doi.org/10.1002/1097-0142(1950)3:1<32::aid-cncr2820030106>3.0.co;2-3.
[27] Ruch Y, Kaeuffer C, Ohana M, Labani A, Fabacher T, Bilbault P, et al. CT lung lesions as predictors of early death or ICU admission in COVID-19 patients. Clin Microbiol Infect 2020;26(10):1417.E5–8. https://doi.org/10.1016/j.cmi.2020.07.030.
[28] Francone M, Iafrate F, Masci GM, Coco S, Cilia F, Manganaro L, et al. Chest CT score in COVID-19 patients: correlation with disease severity and short-term prognosis. Eur Radiol 2020;1. https://doi.org/10.1007/s00330-020-07033-y.
[29] Zhang J, Meng G, Li W, Shi B, Dong H, Su Z, et al. Relationship of chest CT score with clinical characteristics of 108 patients hospitalized with COVID-19 in Wuhan, China. Respir Res 2020;21:180. https://doi.org/10.1186/s12931-020-01440-x.
[30] Zhou S, Wang Y, Zhu T, Xia L. CT features of coronavirus disease 2019 (COVID-19) pneumonia in 62 patients in Wuhan, China. Am J Roentgenol 2020;214:1287–94. https://doi.org/10.2214/AJR.20.22975.
[31] Grillo F, Barisione E, Ball L, Mastracci L, Fiocca R. Lung fibrosis: an undervalued finding in COVID-19 pathological series. Lancet Infect Dis 2021;21(4). e72. https://doi.org/10.1016/S1473-3099(20)30582-X.
[32] Widders A, Broom A, Broom J. SARS-CoV-2: the viral shedding vs infectivity dilemma. Infect Dis Heal 2020;25:210–5. https://doi.org/10.1016/j.idh.2020.05.002.
[33] Lin A, He ZB, Zhang S, Zhang JG, Zhang X, Yan WH. Early risk factors for the duration of SARS-CoV-2 viral positivity in COVID-19 patients. Clin Infect Dis 2020;71(16):2061–5. https://doi.org/10.1093/cid/ciaa490.
[34] Vena A, Taramasso L, Di Biagio A, Mikulska M, Dentone C, De Maria A, et al. Prevalence and clinical significance of persistent viral shedding in hospitalized adult patients with SARS-CoV-2 infection: a prospective observational study. Infect Dis Ther 2021;10:387–98. https://doi.org/10.1007/s40121-020-00381-8.
[35] van Kampen Jja, van de Vijver DAMC, Fraaij PLA, Haagmans BL, Lamers MM, Okba N, et al. Duration and key determinants of infectious virus shedding in hospitalized patients with coronavirus disease-2019 (COVID-19). Nat Commun 2021;12. https://doi.org/10.1038/s41467-020-20568-4.